ADVANCED FUNCTIONAL MATERIALS
www.afm-journal.de

Catalyst-Free GaN Nanorods Synthesized by Selective Area Growth

*Yen-Ting Lin, Ting-Wei Yeh, Yoshitake Nakajima, and P. Daniel Dapkus**

GaN nanorod formation on Ga-polar GaN by continuous mode metalorganic chemical vapor deposition selective area growth (MOCVD SAG) is achieved under a relatively Ga-rich condition. The Ga-rich condition, provided by applying a very low V/III ratio, alters the growth rates of various planes of the defined nanostructure by increasing relative growth rate of the semi-polar tilted m-plane {1–101} that usually is the slowest growing plane under continuous growth conditions. This increased growth rate relative to the non-polar m-plane {1–100} and even the c-plane (0001), permits the formation of GaN nanorods with nonpolar sidewalls. In addition, a new growth mode, called the NH_3-pulsed mode, is introduced, utilizing the advantages of both the continuous mode and the lower growth rate pulsed mode to form nanorods. Finally, nanorods grown under the different growth modes are compared and discussed.

1. Introduction

GaN nanorods have gained substantial interest because of their potential applications in devices such as light emitting diodes,[1–5] laser diodes[6] and transistors for power electronics.[7] The small foot print of the nanorod reduces the threading dislocation density[8] in homoepitaxial growth through spatial filtering and dislocation bending and relieves the strain due to the thermal expansion and lattice mismatch in heteroepitaxial growth. InGaN/GaN based LED structures formed by the growth of InGaN quantum wells (QWs) on the side wall of the nanorod is an especially promising structure to explore to solve the persistent "efficiency droop" problem observed in most LEDs formed on the c-plane. The large surface area of the active region can effectively decrease the operating current density hence alleviating the droop effect. In addition, the elimination of piezoelectric field inside the QWs on the non-polar sidewalls allows a thicker quantum well to be formed and in turn reduces the leakage current and increases the radiative recombination efficiency.[9,10] In order to form a uniform and reproducible nanorod array for high quality LED devices, it is important to find an adequate epitaxial method for their growth and to understand the physical mechanisms underlying their formation.

GaN nanorod arrays have been grown by the vapor–liquid–solid (VLS) growth,[11,12] molecular beam epitaxy (MBE)[13] and metalorganic chemical vapor deposition (MOCVD).[14–17] In the case of catalyst free MOCVD, selective area growth (SAG) epitaxy method is the most common way to produce GaN nanorods by controlling the kinetics of growth on various facets formed during the growth. Li, Bergbauer et al.[15,17] have studied catalyst free MOCVD GaN nanorod growth on sapphire and N-polar GaN. It is well known that under typical MOCVD growth conditions on Ga-polar GaN substrate, selective area growth of GaN nanostructures will predominantly form as nanopyramids. To alter this growth habit, Hersee et al.[8,14] introduced the pulsed growth mode, during which the group V and group III precursors are injected separately in time, and achieved growth of GaN nanorods. Chen et al.[18] and Choi et al.[19] also successfully demonstrated GaN nanorod formation using the continuous growth mode, by controlling the pattern pitch, temperature and V/III molar ratio.

The mechanisms of nanorod growth by the pulsed mode have been discussed,[20] but the mechanism for the continuous growth mode has not been described. In this paper, the GaN nanorod formation by continuous growth mode as well as the principles behind their formation will be discussed. In addition, a comparison will be made between nanorods grown under different growth modes. The paper is organized in the following manner: We first designed a series of experiments to study GaN nanostructure formation and growth behavior by manipulating the V/III molar ratio and the growth temperature. We then investigate their formation mechanism and characterize the as-grown nanorods' optical response by cathodoluminescence (CL). Based on the characteristics of the pulsed growth and continuous growth modes, we investigate a new growth mode, the NH_3-pulsed growth mode, to improve the nanorods. Finally, a comparison of these different growth modes and the properties of materials grown by each are discussed.

Y.-T. Lin, Dr. T.-W. Yeh, Y. Nakajima, Prof. P. D. Dapkus
Center for Energy Nanoscience
University of Southern California
Los Angeles, CA 90089, USA
E-mail: dapkus@usc.edu
Y.-T. Lin, Y. Nakajima, Prof. P. D. Dapkus
Ming Hsieh Department of Electrical Engineering
University of Southern California
Los Angeles, CA 90089, USA
Dr. T.-W. Yeh, Prof. P. D. Dapkus
Mork Family Department of Chemical Engineering and Materials Science
University of Southern California
Los Angeles, CA 90089, USA

DOI: 10.1002/adfm.201303671

Table 1. Experiments details of experimental sets A, B, and C.

Experimental set	Temperature [°C]	TMG carrier gas flow rate [sccm][a)]	NH_3 flow rate [sccm][b)]
A	1125	24	5–150
B	1125	8–48	5
C	1050–1175	36	5

[a)]1 sccm of TMG carrier gas flow results in a delivery of 2.2 μmol min^{-1}. of TMG under the conditions employed; [b)]1 sccm of NH_3 flow equals 44.66 μmol min^{-1}.

2. Experiments Details for Continuous Growth Mode

In the continuous growth experiments described here, we apply MOCVD growth using a variety of growth conditions to selected area growth (SAG) on a nanopatterned substrate. The sample preparation and the experimental procedures can be found in our previous work.[20] Based on our observations in studying pulsed mode processes, we extended our growth method toward continuous mode by decreasing the V/III molar ratio and increasing the growth temperature compared to those we applied in the pulsed mode growth studies. We designed 3 sets of experiments summarized in **Table 1**. The total pressure is set to be 250 Torr and nitrogen is used as the carrier gas. In all cases, note that the relative partial pressure of the V/III precursors is lower than typically employed in MOCVD growth and in our previous pulsed mode growth studies. After growth, the as-grown GaN nanorods are studied by a high-resolution field-emission scanning electron microscope (FE-SEM) for their profile, transmission electron microscopy (TEM) for their crystal structure and cathodoluminescence (CL) for their optical properties.

3. Results and Discussion of Mechanistic Principles

3.1. Effect of V/III Molar Ratio on Nanostructure Formation

In experiment set A, the temperature and TMG flow rate are set at 1125 °C and 24 sccm respectively, while the NH_3 flow rate is varied from 150 sccm to 5 sccm. The nanostructure morphology evolution as a function of NH_3 flow rate can be seen in **Figure 1**a: 150; b: 25; c: 10; and d: 5 sccm. The result shows that the nanopyramid structure defined by {1–101} semipolar planes is formed when the NH_3 partial pressure is high (Figure 1a)). The size of the nanopyramids is comparable to the original opening diameter indicating that the growth rate of semipolar m-plane {1–101} is extremely low and limits the formation of nanostructures as nanopyramids. The slow growth rate of these planes has been attributed to a hydrogen-passivation effect,[21,22] where the decomposition of NH_3 acts as the sources of hydrogen atoms that attach to the surface bonding sites. When the NH_3 injection rate is decreased to 25 sccm, we see that the pyramids become larger and less symmetric, and some of the nanostructures become a tetrahedral shape. This trend indicates that the {1–101} planes start to become

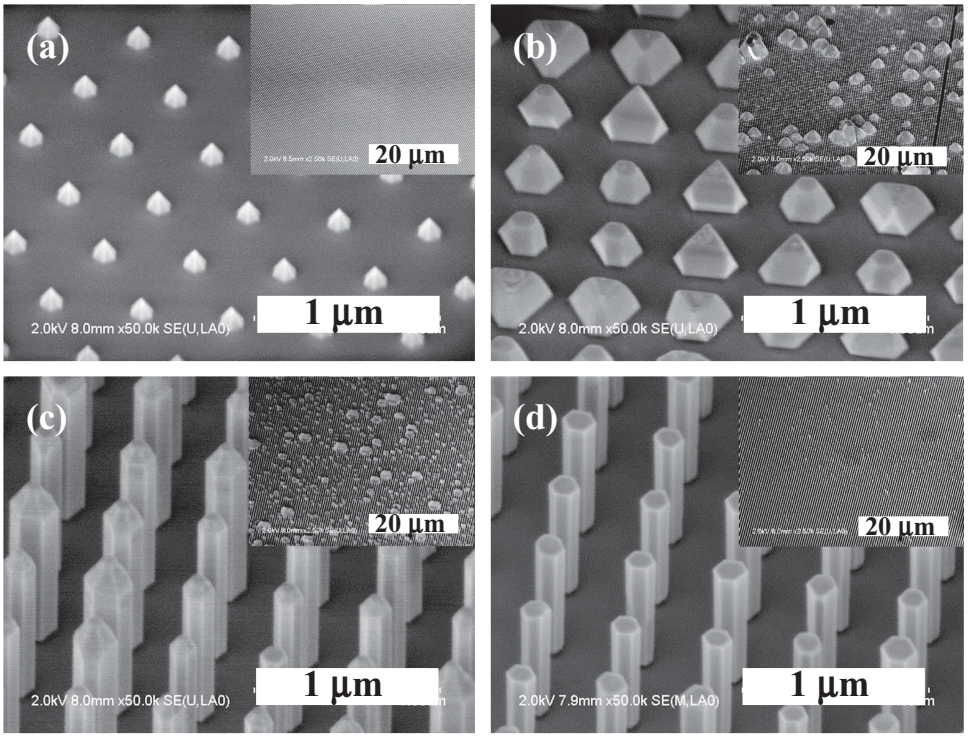

Figure 1. Experiment set A: Nanostructure evolution with respect to NH_3 flow rate a) 150; b) 25; c) 10; and d) 5 sccm, which are taken under a magnification of 50K. Inset figures are the lower magnification images of the arrays at the corresponding NH_3 flow rate.

Table 2. Nanorod array uniformity comparison under growth conditions with different V/III molar ratio.

TMG flow rate [sccm]	V/III molar ratio	Growth time [s]	Measured average nanorod height [nm] / standard deviation	Measured average nanorod width [nm]/standard deviation
8	12.6	1800	948 / 58.6	179/22.2
12	8.4	1200	874 / 43.6	166/21.0
24	4.2	300	1077 / 23.9	146/5.9
48	2.1	150	943 / 15.7	130/7.3

unstable at lower NH_3 partial pressure since the concentration of hydrogen surface species that passivate the surface has been replaced by Ga and the growth of these planes is triggered. At still lower NH_3 flow rates (10 sccm), the growth of the {1–101} planes increase and rod formation is achieved. Finally when NH_3 flow rate is only 5 sccm, the rods become thinner and shorter indicating an insufficiency of NH_3, meanwhile, the top of the rod becomes flat indicating that the relative growth rate of {1–101} plane is even higher than that of c-plane.

In experiment set A, we found that a lower NH_3 injection rate not only promotes nanorod formation but improves the uniformity of the nanostructure arrays as well. To further investigate the effect of V/III molar ratio on the nanorod profiles, we maintain the NH_3 flow at 5 sccm and adjust the TMG flow rate from 8 sccm to 48 sccm during the growth, as presented in experiment set B. Each sample is grown for a different duration scaling the TMG flow rate to achieve the same growth rate and a nominal height of 1 um. After growth, the as-grown nanorod arrays are examined by FE-SEM and the rod profile is characterized by image processing software to obtain the size of individual nanorods. The growth time versus TMG injection rate and the statistical data on the physical dimension of the nanorods (70 nanorods' profile are collected) is summarized in **Table 2**, the SEM images are shown in **Figure 2** with a V/III molar ratio a: 12.6; b: 8.4; c: 4.2; and d: 2.1 respectively, and the histograms of the nanorods profile distributions are shown in **Figure 3**a) height and 3b) width. The SEM image of the patterned substrate and its opening size distribution are also shown in Figure 3c,d.

From the nanorod profile distribution shown in Figure 3 we can clearly see that the nanorod array uniformity improves with a lower V/III molar ratio. The nanorod array uniformity is limited by the size distribution of the openings on the patterned substrate and therefore the array uniformity does not improve at a even lower V/III molar ratio (2.1). Besides, a reduction of average nanorod width at lower V/III molar ratio is observed. This indicates that lower V/III molar ratio promotes vertical growth of nanorods and is consistent with the phenomena observed in previous studies of the pulsed growth mode.[20]

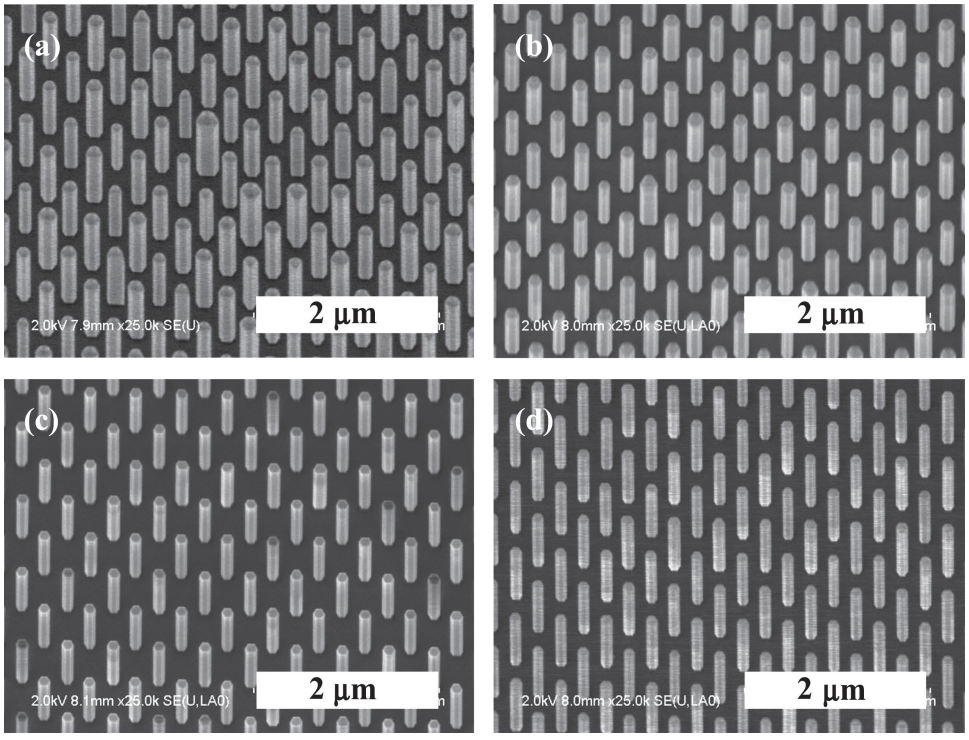

Figure 2. Experimental set B: Rod morphology with V/III molar ratio equal to a) 12.6; b) 8.4; c) 4.2; and d) 2.1. (Figure 2c is taken at a 20 degree bird's eye view while the rest are at 30 degrees.)

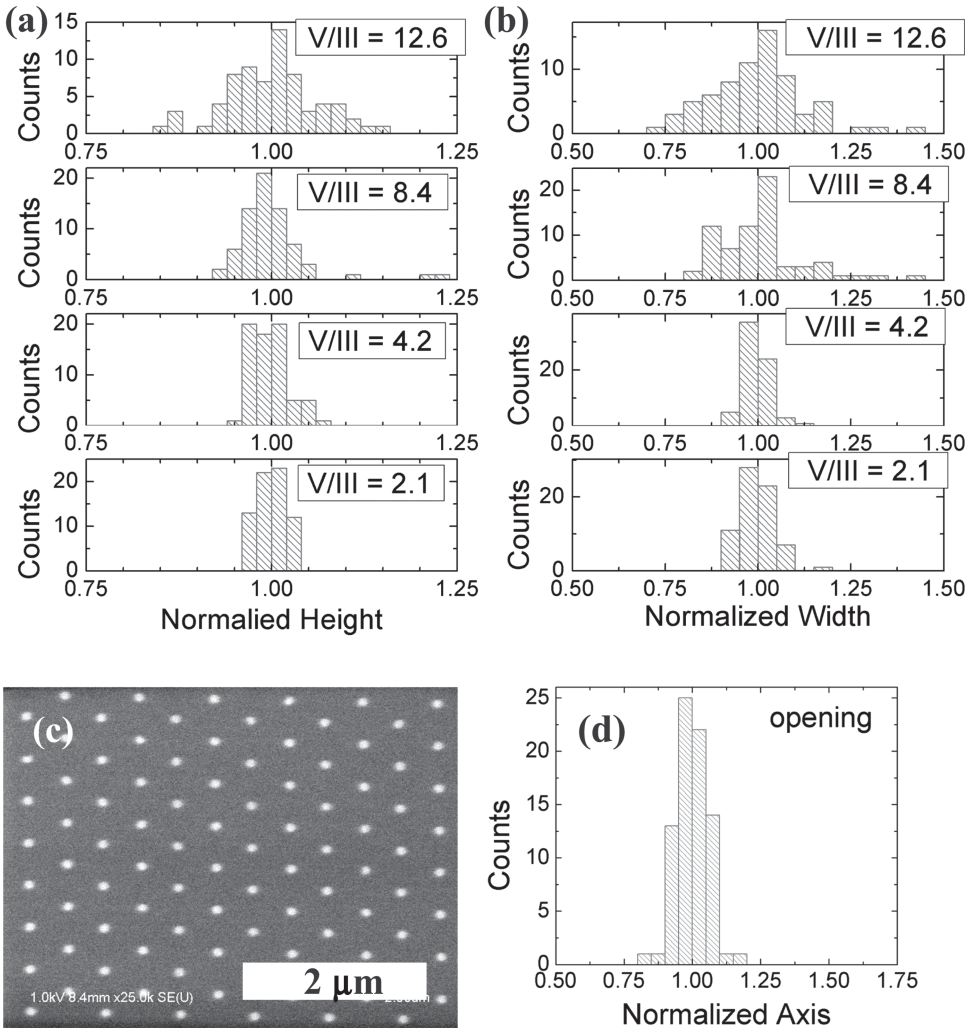

Figure 3. Histogram of 70 nanorods' profile distribution of a) normalized height; and b) normalized width. c) SEM image of patterned substrate and d) its opening size distribution.

3.2. Effect of Growth Temperature

It has been shown that the V/III molar ratio plays a critical role in nanorod formation in the continuous growth mode. In experimental set C we will study the effect of growth temperature. The nanorod profile evolution as a function of growth temperature is shown in **Figure 4**a: 1050; b: 1085; c: 1125; and d: 1175 °C. When the temperature is low (Figure 4a), though the nanostructure forms as a nanorod, the uniformity of the nanorod array is poor with severe parasitic growth. In addition, the sharpness of the nanorod top indicates that the growth rate of {1–101} is smaller than that of the c-plane, even though the V/III molar ratio is sufficiently low to allow nanorod formation. As the growth temperature increases (Figure 4b), the vertical-to-lateral aspect ratio of nanorods becomes larger, the nanorod array uniformity improves and the amount of parasitic growth is reduced as well. When the growth temperature reaches 1125 °C (Figure 4c), we see a fairly uniform nanorod array free of parasitic growth, and the flat top of nanorod indicates at this temperature the growth rate of {1–101} has exceeded that of c-plane. Finally, when the temperature is further increased to 1175 °C (Figure 4d), thermal etching and Ga desorption effects become much more significant and the nanostructure formation is unstable under such growth conditions. Our results agree with previous experimental reports,[20,23,24] where a lower growth rate of m-plane is observed at a higher growth temperature.

3.3. Discussion of the Nanorod Formation

As presented in experimental set A and B, two phenomena are observed in the nanostructure evolution with respect to V/III molar ratio: the nanorod formation (as a consequence of growth rate variation among the various planes) and the improvement of array uniformity. As shown in Figure 1, the shape of the nanostructure evolves from a nanopyramid to a nanorod, and the uniformity of the nanostructure array

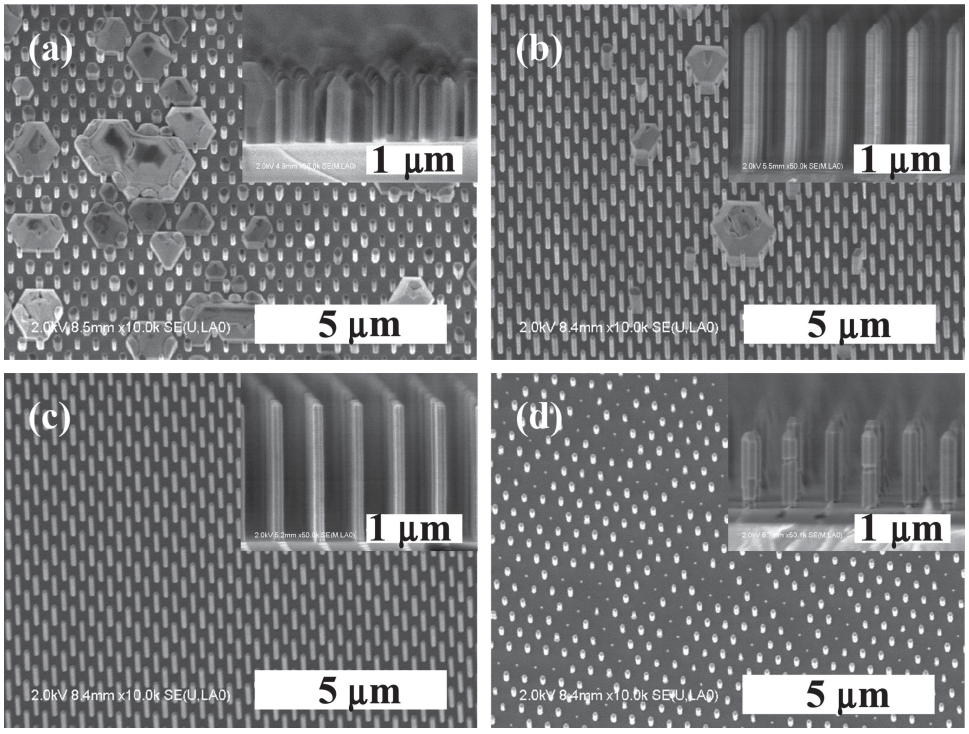

Figure 4. Bird's eye view (20 degree) SEM image of Nanorod array grown by continuous growth mode under different growth temperature a) 1050; b) 1085; c) 1125; and d) 1175 °C. The nanorod profile evolution as a function of growth temperature can be seen in the inset figures.

improves when NH_3 flow rate decreases from 150 to 5 sccm. These facts indicate that the formation of the nanostructure is the result of not only the relative growth rate between various planes, but their absolute growth rate as well. When NH_3 injection rate is high (150 sccm), only c-plane growth is observed which causes the structure to self-limit owing to the low growth rate of the {1–101} planes, and the volume of the nanostructure is much smaller than that grown under a much lower NH_3 flow rate (10 sccm). This phenomenon reflects the fact that the growth of {1–101} plane is not only relatively low, but also absolutely low. The low growth rate can be attributed to the so-called "hydrogen-passivation" effect[21,22] where the hydrogen atoms tend to bond with the nitrogen atoms on the N-terminated surface, such as {1–101} and (000–1) planes, therefore insulating these surfaces from growth ambient and in turn slowing down and even stopping the growth of them. This is always noted in kinetic studies of facet formation by a deep notch that always manifests itself in a kinetic Wulff's plot.[23,25] It is well known that the thermal decomposition process of NH_3 will release hydrogen atoms that limit the growth rate on the {1–101} planes. Therefore, in order to alleviate this effect, a very low V/III ratio must be applied. The alleviation of hydrogen-passivation effect can be clearly observed if we compare the volume of the nanostructures in Figure 1. The Ga incorporation rate under a 150 sccm injection of NH_3 is only a small fraction (≈4.3% in volume ratio) of that under a 10 sccm NH_3 injection. As NH_3 injection rate decreases from 150 to 25 sccm, the nanopyramid becomes larger, and the m-plane appears, which indicate that the growth rate of {1–101} plane increases due to the reduced NH_3 flow. At this NH_3 injection rate we can see that the corresponding nanostructure has a pyramid-like but irregular shape (Figure 1b), also from the inset figure, parasitic growth (which is absent under 150 sccm NH_3 flow rate, as shown in the inset of Figure 1a with a much larger size than that of the nanostructure itself can be observed throughout the growth area. Since a reduced NH_3 flow rate will release parts of the semipolar planes from hydrogen-passivation effect and allows these nanostructures to grow much faster than those with passivated planes and therefore the uniformity of the nanostructure array becomes poor. As the NH_3 flow is further decreased from 25 to 10 sccm, we see nanorod formation is achieved which implies that the growth rate of {1–101} planes becomes much faster than that of m-plane, and is comparable to that of the c-plane. Parasitic growth becomes denser and with smaller volume compared to those in Figure 1b, which also indicates that growth of nanorods at growth sites becomes favorable and the uniformity of the nanorod array becomes better as well. Finally, at a 5 sccm NH_3 injection rate, the hydrogen-passivation effect almost disappears due to a very low V/III ratio, and the {1–101} planes become growth favorable planes so that their growth rate is even higher than that of c-plane, as implied by the fact that the top of the nanorod becomes flat. In addition, the field of nanorod array possesses a much better uniformity as well as being free of parasitic growth. The control of the NH_3 flow rate not only changes the nanostructure profile, but also influences their overall uniformity. Since at a higher NH_3 flow rate (>10 sccm), the hydrogen-passivation effect plays a dominant role in the nanostructures formation, therefore only part of the nanostructures are able to grow. The random distribution of these favorable and unfavorable nanostructures

therefore renders poor uniformity to the overall array. When the NH_3 flow rate is sufficiently low (< 10 sccm) such that the nanostructures are totally free from the growth limitations on the {1–101} planes imposed by the hydrogen-passivation effect, the growth of the nanostructure array becomes mass transport limited. Since the diffusion length of the mass transport region (tens of micrometers[26,27] or even higher at higher temperature and lower V/III molar ratio in our case) is much larger than the size of the nanorod and the pitch of the array, the local nanorod array will have a much better uniformity than those grown under kinetic limited condition. In short, a mass transport limited condition, which can be achieved by applying lower V/III molar ratio, is able to produce a nanorod array with better uniformity.

Experimental set B provides a clearer view of how V/III molar ratio affects the adatom kinetics during the growth and therefore the nanorod array uniformity. As discussed above, at a lower V/III molar ratio the nanorods are grown under a situation away from the kinetic-limited condition and the growth of {1–101} plane becomes highly favorable as this crystallographic surface has much lower surface formation energy than {1–100} planes and even the (0001) plane.[22,28] The high growth rate of {1–101} and (0001) planes not only makes the growth conditions strongly mass-transport limited and therefore improves the uniformity of nanorod array, but increases the vertical-to-lateral growth ratio of nanorods as well.

The kinetics of growth were investigated by Lymperakis and Neugebauer[29] who performed calculations that showed a large anisotropic diffusion path barrier for Ga adatoms on the GaN m-plane. That is, the diffusion barrier along the <0001> direction is much larger than that toward <11–20> direction. Therefore, some of the Ga adatoms landing on the sidewalls of the nanostructures are unable to reach the top of them at lower growth temperature which not only reduces the vertical growth but contributes to lateral growth as well. Besides, as suggested by Sawicka et al.,[30] a N-rich condition will be required in order to form a smooth m-plane, while a Ga-rich condition must be applied for nanorod formation under continuous growth mode. In this case, the undesorbed Ga species which are unable to reach the top region of nanorods cannot contribute to a smooth lateral growth, possibly contributing tosignificant parasitic growth as can be clearly seen in Figure 4a,b.

3.4. Structure and Optical Characterization

The as-grown continuous mode nanorod is examined by transmission electron microscopy (TEM) and cathodoluminescence (CL) for its structural and optical characterization. The TEM image of nanorod grown by continuous growth mode is shown in **Figure 5** which is taken along the <11–20> zone axis, where the diffraction pattern (Figure 5c) indicates the wurtzite structure of the nanorod. No stacking faults or dislocations are found within the nanorod, as is the case for nanorod grown under pulsed growth mode.[3]

For CL characterization, we compare the spectra of undoped nanorods grown under different V/III ratioes (2.1 and 8.4) as well as un-doped and Si-doped nanorods (both rods are grown

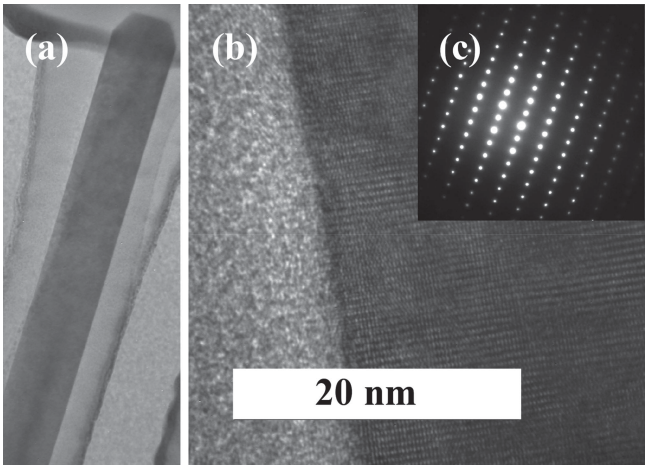

Figure 5. TEM image of nanorod grown by continuous growth mode. The nanorod is taken along <11–20> zone axies (Figure 5b), and the diffraction pattern indicates a wurtzite structure (Figure 5c). The nanorod is free from twins, stacking faults and threading dislocations (Figure 5a).

under V/III equal to 2.1), as shown in **Figure 6**a,b. It can be seen that the yellow-luminescence (YL) to band-edge emission intensity ratio is much larger for nanorods grown at a lower V/III ratio than at a higher V/III ratio condition. The latter spectrum is similar to a CL spectrum measured for bulk epitaxial GaN layers grown by MOCVD (Figure 6c). There is almost no difference in the emission spectrum between the rods grown with and without Si-doping (Figure 6b). The origin of YL has been attributed to multiple physical origins.[31] Carbon impurities on nitrogen sites have been implicated in a number of different studies.[32–35] The dominance of the YL under low V/III ratios is consistent with such a model since incomplete removal of C from precursor fragments and the occurrence of a higher density of N vacancies would be enhanced by a low V/III ratio. More work is required to investigate the origin of this large YL to band-edge emission intensity ratio in our samples and its effects on the performance of devices that incorporate GaN nanorods grown under such conditions, which beyond the scope of this paper.

Though the continuous mode nanorods exhibit an abnormal luminescence spectrum under CL measurement, the nanorod templates with InGaN multiple quantum wells (MQWs) grown on them do not shown this strong yellow luminescence under photoluminescence (PL) measurement, as shown in Figure 6d. The emission peak from the MQWs is designed to be centered around 410 nm to prevent overlapping with the YL emission. The MQWs growth condition can be found elsewhere.[3] We speculate that suppression of YL band luminescence in the PL spectra of nanorods with MQW shells arises because the inner core of the structure is not excited by the incident laser light. The high absorption coefficient of the InGaN/GaN MQW at the wavelength of the excitation laser may preclude the core from being excited. Also the small size of the nanorod may allow the carriers that are created there to diffuse to the MQWs region before they are trapped by the defects inside the nanorods templates. More work is required to clarify these speculations.

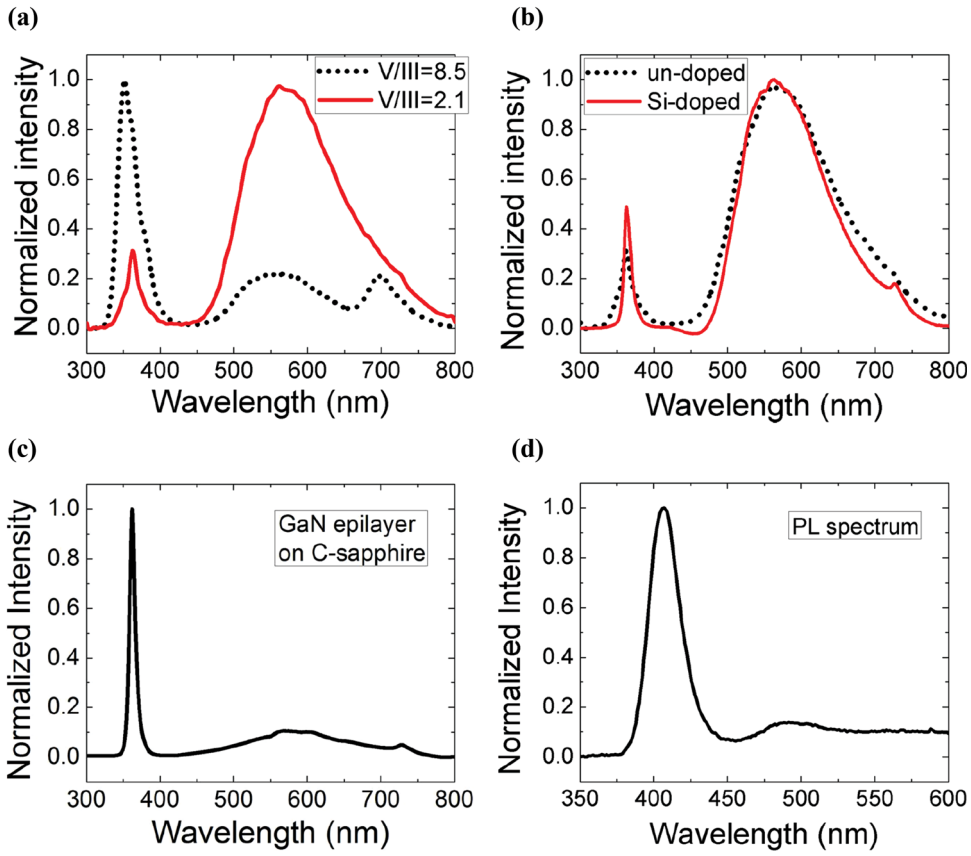

Figure 6. a) CL spectrum of nanorod grown under 2 different V/III ratio (8.4 and 2.1 by changing TMG flow rate, both are un-doped). b) CL spectrum of nanorod grown with and without Si-doped (V/III ratio is 2.1 in both case). c) CL spectrum of GaN substrate. d) PL spectrum of continuous mode nanorods with InGaN MQWs.

4. The NH_3-pulsed Growth Mode

From the previous discussions it is shown that a Ga-rich and mass transport limited growth condition is required for GaN nanorod formation. These conditions are achieved by injecting the group V and group III source separately in the pulsed growth mode, and by applying a very low V/III molar ratio in the continuous growth mode. Though both growth modes can successfully achieve nanorod formation, they have corresponding problems.

The continuous mode employs a much simpler growth process and has relatively high growth rate, however the nanorods grown under continuous mode exhibit an abnormal emission spectrum, which will be discussed in the next section. Though the pulsed mode is able to produce GaN nanorods with reduced YL band emission, the growth process is complicated since many parameters are involved. Here we introduce a growth mode that we will refer to as the NH_3-pulsed mode, which adopts a simpler growth process than pulsed mode (as shown in **Figure 7**) and is able to achieve GaN nanorods with reduced YL band emission. In this growth mode, only NH_3 flow is pulsed while the injection of TMG is continuous resulting in better utilization of TMG than in the pulsed mode.

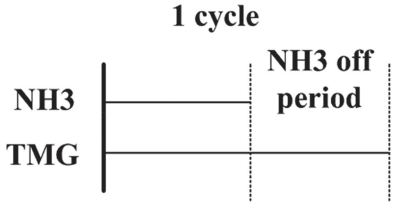

Figure 7. Growth process of NH_3-pulsed mode where only the injection of NH_3 is pulsed.

To achieve the nanorod formation and good array uniformity, the NH_3 flow rate and NH3 off time must be carefully designed. In experimental set D we change the NH_3 flow rate (15–50 sccm) and adjust the NH_3 off time (1–3 s, 8 s for a cycle), while maintaining the temperature at 1125 °C (the same as continuous growth mode) and TMG flow rate at 8 sccm. The morphology of the nanostructure as a function of NH_3 flow rate and off time is shown in **Figure 8**.

The nanorod profile results in experimental set D can be roughly grouped into 3 regions (I), (II), and (III) as indicated in Figure 8a–c,e, and 8f,g, respectively. In region (I) where NH_3 injection rate is still high and NH_3 off period is short,

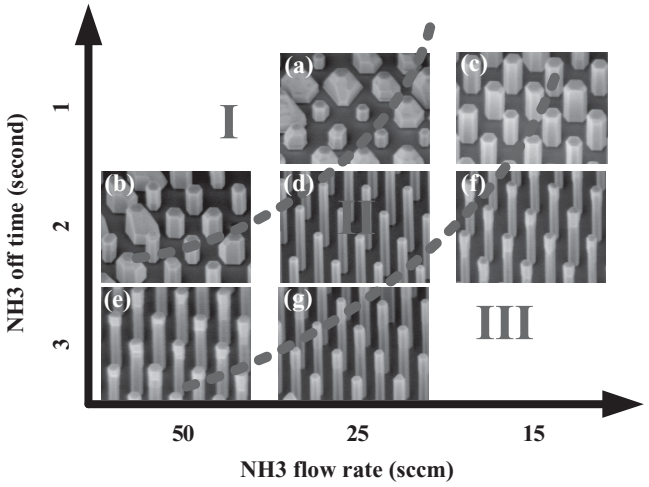

Figure 8. Nanorod profile as a function of NH_3 flow rate and NH_3 off time (8 seconds per cycle).

the overall growth condition is still not favorable for nanorod formation. On the other hand in region (III), the NH_3 injection rate becomes too low and the NH_3 off period is too long. In this region an unusual phenomenon of nanorod structure, a "step" like formation, can be observed on the top part of the nanorod, that will be discussed later. Only under the conditions of region (II) where a moderate NH_3 flow rate and NH_3 off time are applied can the formation of the desired nanorod structure be achieved. At this particular growth temperature and these cycle durations, the locally optimized growth condition for nanorod (Figure 8d) in our system is set at a NH_3 injection rate equal 25 sccm and off time equal 2 s. The SEM image of nanorod array grown by NH_3-pulsed mode as well as nanorod array uniformity histogram (compared with the case under continuous growth mode at V/III equal 2.1) are shown in **Figure 9**a–c, respectively. The pulsed NH3 mode clearly generates high aspect ratio uniform nanorods by controlling the Ga surface kinetics.

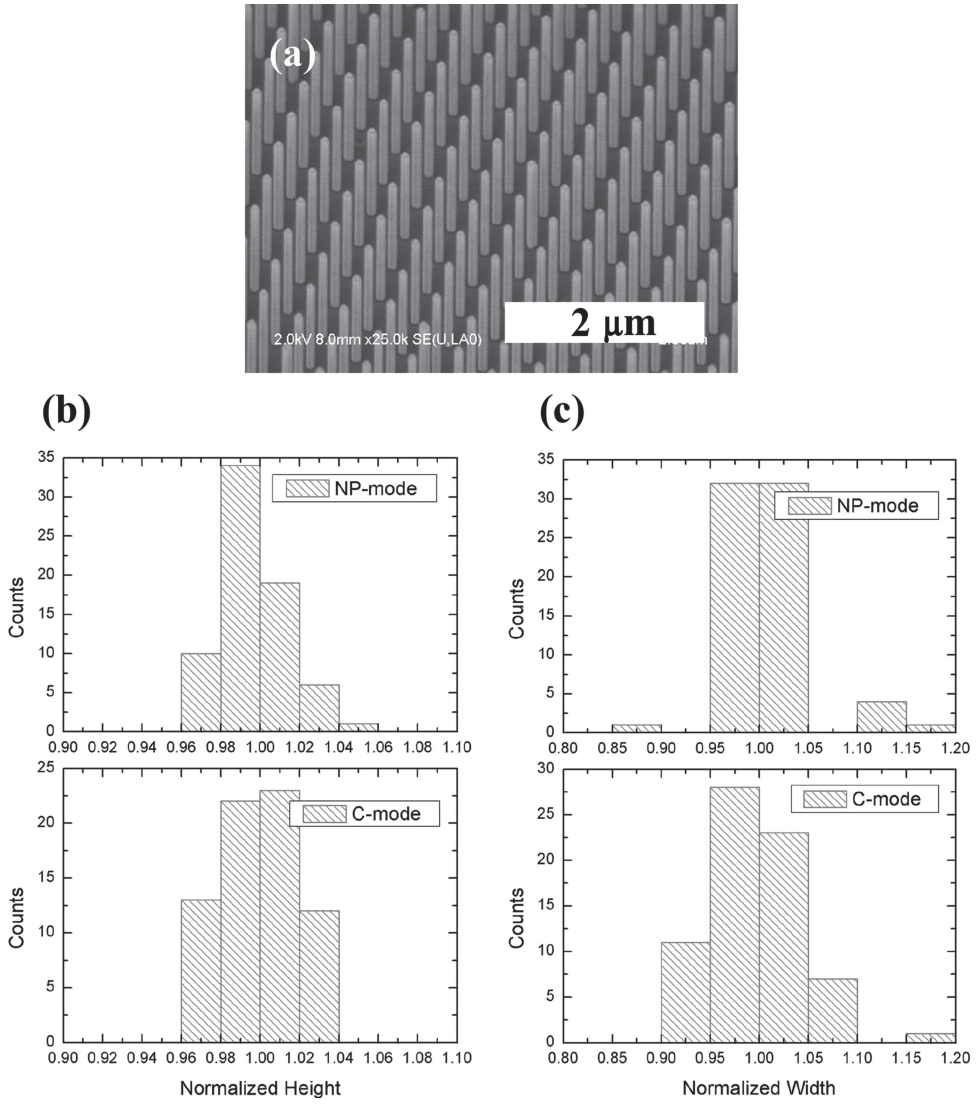

Figure 9. a) Birds-eye view (45 degree) SEM image of nanorod array grown by NH_3-pulsed mode. b,c) Normalized height/Width histogram of nanorod grown by NH_3-pulsed mode (NP-mode, un-doped) and continuous mode (C-mode, V/III = 2.1, un-doped).

Table 3. Comparison between nanorods grown by different growth modes.

Growth mode	Growth rate [nm h^{-1}]	Array uniformity	CL spectrum
Pulsed	1 um	Good	Comparable band-edge and YL emission intensity
NH_3-pulsed	6 um	Good	Large band-edge to YL emission intensity ratio
Continuous	4–20 um[a)]	Good[b)]	Large YL to band-edge emission intensity ratio

[a)]The growth rate of nanorod by continuous mode can be enhanced by increasing TMG injection rate while it is more complicated in pulsed and NH_3-pulsed mode; [b)]Over 24 sccm TMG injection rate (V/III molar ratio equal 4.2) is required to obtain good uniformity of nanorod array in continuous mode.

The step-like growth on the top of the nanorods shown in region (III), is similar to a phenomena observed by Galopin et al.[36] In their study a step-like growth was attributed to GaN nucleation at the junction of the nanorod base region and the substrate, rather than the nucleation directly on the sidewall of the nanorod. The step growth is believed to start from the bottom of the nanorod and is parallel to the nanorod growth direction. In our case, the steps seem to nucleate from the top of the nanorod and then grow toward the bottom of the nanorod. The origin of the step growth, which might provide a clue for a more detailed nanorod formation mechanism, is still unclear but it is obviously related to the NH_3 injection condition which controls the growth kinetics of various planes of the nanorod. More work is required to clarify this phenomenon.

5. Nanorod Comparison by Different Growth Mode

In the previous sections we have discussed and characterized nanorods grown by the continuous mode and NH_3-pulsed mode. In this section, we provide a comparison between the growth rates, uniformities, and emission spectra of optimized nanorods grown under the various modes. (**Table 3**) The CL spectra of nanorods are shown in **Figure 10**a: pulsed; b: NH_3-pulsed; and c: continuous mode. Note that only the continuous mode nanorods exhibit a strong YL. The PL spectra of InGaN MQWs grown on each mode nanorods template are also shown in **Figure 11**a: pulsed; b: NH_3-pulsed; and c: continuous mode.

6. Summary

In this paper, we achieve GaN nanorod growth on Ga-polar substrate by continuous growth mode and discuss the operable growth mechanisms in their formation. A low V/III molar ratio and high growth temperature favor the growth of {1–101} planes and therefore are critical for nanorod formation as well as achieving good array uniformity. The continuous mode is simpler to implement than pulsed modes but the nanorods produced by continuous mode exhibit an abnormal emission spectrum with strong YL band emission which may result from impurity induced emission. The NH_3-pulsed mode combines some advantages of both the continuous and pulsed growth mode was discussed. This mode can be used to grow nanorods with a relatively high growth rate while achieving low deep state luminescence emission. We have also compared the different growth modes with respect to the nanorod profile, luminescence property as well as the emission of InGaN MQWs that

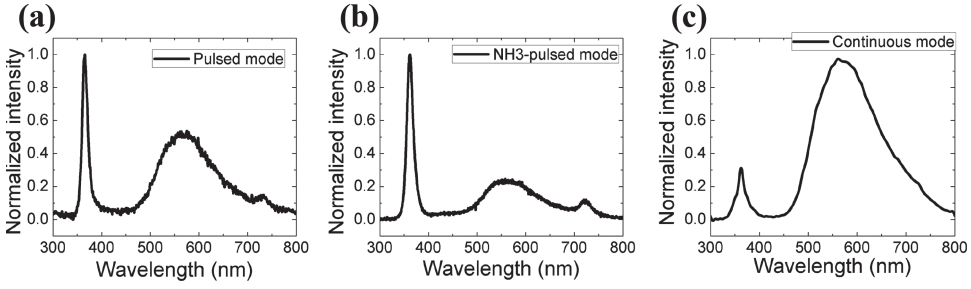

Figure 10. CL spectrum of nanorods grown by a) pulsed; b) NH_3-pulsed; and c) continuous (V/III = 2.1) mode.

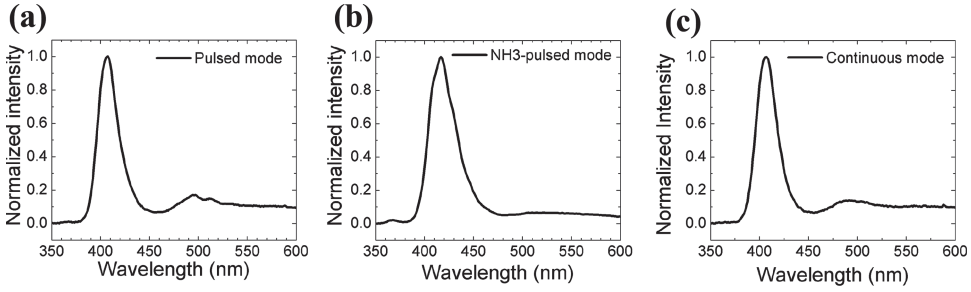

Figure 11. PL spectrum of InGaN MQWs grown on different mode nanorods template by a) pulsed; b) NH_3-pulsed; and c) continuous (V/III = 2.1) mode.

utilize these nanorod templates. Based on the various advantages of these growth modes, we can now adopt the appropriate growth mode for different nanotechnology applications.

Acknowledgement

This work was supported in part by the Center for Energy Nanoscience, an Energy Frontier Research Center funded by the U.S. Department of Energy, Office of Basic Energy Sciences under Award Number DE-SC0001013 (Y.T.L., Y. N., and P.D.D.) and by NSF through Award ECS-0507270 (T.W.Y. and P.D.D.)

Received: October 28, 2013
Revised: December 12, 2013
Published online: February 10, 2014

[1] Z. Zhong, F. Qian, D. Wang, C. Lieber, *Nano Lett.* **2003**, *3*, 343.
[2] S. D. Hersee, M. Fairchild, A. K. Rishinaramangalam, M. S. Ferdous, P. M. V. L. Zhang, B. S. Swartzentruber, A. A. Talin, *Electron. Lett.* **2009**, *45*.
[3] T.-W. Yeh, Y.-T. Lin, L. S. Stewart, P. D. Dapkus, R. Sarkissian, J. D. O'Brien, B. Ahn, S. R. Nutt, *Nano Lett.* **2012**, *12*, 3257.
[4] H. Sekiguchi, K. Kishino, A. Kikuchi, *Appl. Phys. Lett.* **2010**, *96*, 231104.
[5] Y. J. Hong, C.-H. Lee, A. Yoon, M. Kim, H.-K. Seong, H. J. Chung, C. Sone, Y. J. Park, G.-C. Yi, *Adv. Mater.* **2011**, *23*, 3284.
[6] S. Gradečak, F. Qian, Y. Li, H.-G. Park, C. M. Lieber, *Appl. Phys. Lett.* **2005**, *87*, 173111.
[7] Y. Huang, X. Duan, Y. Cui, C. M. Lieber, *Nano Lett.* **2002**, *2*, 101.
[8] S. D. Hersee, A. K. Rishinaramangalam, M. N. Fairchild, L. Zhang, P. Varangis, *J. Mater. Res.* **2011**, *26*, 2293.
[9] S.-C. Ling, T.-C. Lu, S.-P. Chang, J.-R. Chen, H.-C. Kuo, S.-C. Wang, *Appl. Phys. Lett.* **2010**, *96*, 231101.
[10] C.-H. Chiu, D.-W. Lin, C.-C. Lin, Z.-Y. Li, W.-T. Chang, H.-W. Hsu, H.-C. Kuo, T.-C. Lu, S.-C. Wang, W.-T. Liao, T. Tanikawa, Y. Honda, M. Yamaguchi, N. Sawaki, *Appl. Phys. Express* **2011**, *4*, 012105.
[11] X. Duan, C. M. Lieber, M. J. J. A. Phys, *J. Am. Chem* **2000**, *122*, 188.
[12] T. Kuykendall, P. Pauzauskie, S. Lee, Y. Zhang, J. Goldberger, P. Yang, *Nano Lett.* **2003**, *3*, 1063.
[13] M. a. Sanchez-Garcia, E. Calleja, E. Monroy, F. J. Sanchez, F. Calle, E. Muñoz, R. Beresford, *J. Cryst. Growth* **1998**, *183*, 23.
[14] S. Hersee, X. Sun, X. Wang, *Nano Lett.* **2006**, *6*, 1808.
[15] W. Bergbauer, M. Strassburg, C. Kölper, N. Linder, C. Roder, J. Lähnemann, A. Trampert, S. Fündling, S. F. Li, H.-H. Wehmann, A Waag, *Nanotechnology* **2010**, *21*, 305201.
[16] R. Koester, J. S. Hwang, C. Durand, D. L. S. Dang, J. Eymery, *Nanotechnology* **2010**, *21*, 015602.
[17] S. F. Li, S. Fuendling, X. Wang, S. Merzsch, M. a. M. Al-Suleiman, J. D. Wei, H.-H. Wehmann, A. Waag, W. Bergbauer, M. Strassburg, *Cryst. Growth Des.* **2011**, *11*, 1573.
[18] X. J. Chen, B. Gayral, D. Sam-Giao, C. Bougerol, C. Durand, J. Eymery, *Appl. Phys. Lett.* **2011**, *99*, 251910.
[19] K. Choi, M. Arita, Y. Arakawa, *J. Cryst. Growth* **2012**, *357*, 58.
[20] Y.-T. Lin, T.-W. Yeh, P. D. Dapkus, *Nanotechnology* **2012**, *23*, 465601.
[21] R. M. Feenstra, Y. Dong, C. D. Lee, J. E. Northrup, *J. Vac. Sci. Technol. B* **2005**, *23*, 1174.
[22] T. Akiyama, D. Ammi, K. Nakamura, T. Ito, *Phys. Rev. B* **2010**, *81*, 245317.
[23] V. Jindal, F. Shahedipour-Sandvik, *J. Appl. Phys.* **2009**, *106*, 083115.
[24] T. Akasaka, Y. Kobayashi, S. Ando, N. Kobayashi, M. Kumagai, *J. Cryst. Growth* **1998**, *189*, 72.
[25] Q. Sun, C. D. Yerino, T. S. Ko, Y. S. Cho, I.-H. Lee, J. Han, M. E. Coltrin, *J. Appl. Phys.* **2008**, *104*, 093523.
[26] M. E. Coltrin, C. C. Mitchell, *J. Cryst. Growth* **2003**, *254*, 35.
[27] T. Shioda, Y. Tomita, M. Sugiyama, Y. Shimogaki, Y. Nakano, *Jpn. J. Appl. Phys.* **2007**, *46*, L1045.
[28] D. Segev, C. G. Van de Walle, *Surf. Sci.* **2007**, *601*, L15.
[29] L. Lymperakis, J. Neugebauer, *Phys. Rev. B* **2009**, *79*, 241308.
[30] M. Sawicka, H. Turski, M. Siekacz, J. Smalc-Koziorowska, M. Kryśko, I. Dzięcielewski, I. Grzegory, C. Skierbiszewski, *Phys. Rev. B* **2011**, *83*, 245434.
[31] M. a. Reshchikov, H. Morkoç, *J. Appl. Phys.* **2005**, *97*, 061301.
[32] D. S. Green, U. K. Mishra, J. S. Speck, *J. Appl. Phys.* **2004**, *95*, 8456.
[33] C. G. Van de Walle, J. Neugebauer, *J. Appl. Phys.* **2004**, *95*, 3851.
[34] K. Laaksonen, M. G. Ganchenkova, R. M. Nieminen, *J. Phys.: Condens. Matter* **2009**, *21*, 015803.
[35] J. L. Lyons, A. Janotti, C. G. Van de Walle, *Appl. Phys. Lett.* **2010**, *97*, 152108.
[36] E. Galopin, L. Largeau, G. Patriarche, L. Travers, F. Glas, J. C. Harmand, *Nanotechnology* **2011**, *22*, 245606.